

Global Relationships among Physical Properties of Galaxy Cluster Cores*

Yutaka FUJITA[†] and Fumio TAKAHARA

*Department of Earth and Space Science, Graduate School of Science, Osaka University,
Machikaneyama-cho, Toyonaka, Osaka, 560-0043, Japan
E-mail(YF): fujita@vega.ess.sci.osaka-u.ac.jp*

(Received 0000; accepted 0000)

Abstract

Using X-ray data, we investigate interrelations between gas density ρ_0 , virial density ρ_{vir} , core radius R , temperature T , entropy S_{gas} , and metal abundance Z in the core region of clusters of galaxies. First, we confirm that fundamental relations among ρ_0 , R , and T found by Fujita and Takahara are reproduced by another data catalogue. Second, we find that, when clusters have two components in their surface brightness distribution, the inner components also satisfy the same fundamental relations on the assumption that the average temperature of the inner component is the same as that of the outer component. These results strengthen our interpretation that clusters form a two parameter family in terms of mass and ρ_{vir} ; larger ρ_{vir} corresponds to earlier formation epoch. We argue that the inner components represent distinct dark matter components which collapsed ahead of the outer components. Third, we also find a tight relation between S_{gas} and ρ_{vir} both for the outer and inner components; S_{gas} is smaller for larger ρ_{vir} but is larger than that produced through gravitational collapse alone for larger ρ_{vir} . Although radiative cooling affects the thermal evolution, the tight relationship discovered suggests the existence of stable heating sources or stable energy transmission mechanisms. Finally, we find that the iron abundance at the centers of clusters is correlated with ρ_{vir} for the inner components. This implies that iron produced by Type Ia supernovae has more accumulated for clusters formed earlier. We briefly discuss the implications of these findings.

Key words: Cosmology — galaxies: clusters of — galaxies: intergalactic medium — X-rays: general

1. Introduction

Since clusters of galaxies are the largest virialized structure in the universe, they should carry the information on the cosmological structure formation such as the cosmological parameters and the initial density fluctuations. In particular, theoretical studies have shown that the structure of their core region should provide useful clues to these issues. Numerical simulations done by Navarro et al. (1997) demonstrate that the characteristic density of a cluster correlates to that at the formation redshift. By means of a modification of the extended Press & Schechter formalism, Salvador-Solé et al. (1998) show that the core radius of halos is essentially proportional to the virial radius of the clusters at the time of formation. So the cluster cores are expected to retain the properties at the formation epoch rather than to be completely destroyed by subsequent dynamical evolution after the formation. The observations of the central gas density ρ_0 and core radius R are to be compared to these

predictions to give a formation redshift.

Most extensive data sets now available to such studies are X-rays from hot intracluster gas. The X-ray luminosity of clusters L_X is mainly determined by the structure around the core region. The relation between L_X and X-ray temperature T has been used as a diagnostic of cosmological structure formation. However, most of the previous studies have not explicitly cared about the structure of central region, rather they avoided to use physical quantities there. For example, they do not take account of a variation of core radius for a given X-ray temperature. One of the reasons for this is that it was difficult to determine core radii because of their correlation with the slope of surface brightness profile β , the central excess emission (so-called cooling flow), and the poor spatial resolutions of telescopes. However, ROSAT satellite makes it possible to obtain core radii with enough accuracy. Using the data compiled by Mohr et al. (1999), we have investigated the structures in core regions of clusters (Fujita, Takahara 1999a, hereafter Paper I). We find that there are fundamental relations among ρ_0 , R , and T ; clusters are distributed on a band

* OU-TAP 112

† JSPS Research Fellow

in the $(\log \rho_0, \log R, \log T)$ space forming a fundamental plane. Moreover, we find that the observed L_X - T relation is the cross section of the band seen from the main axis of the band, and that the information along the main axis is almost degenerated on the L_X - T relation. By comparing the results with the theoretical predictions, we show that the main axis corresponds to a variation of the central virial density ρ_{vir} and thus to the cluster formation redshift, and that the scatter of the data along it implies a wide range of cluster age (Fujita, Takahara 1999b, hereafter Paper II). In §2 of this paper, we investigate whether these results hold for Einstein data by Jones and Forman (1984), which is another data set giving ρ_0 , R , and T in spite of being less accurate.

The physical nature of the central excess components is another interesting issue. Recently, detailed observations of the central regions also become available thanks to the results obtained with the ASCA satellite, which has an imaging spectroscopic capability for 2-10 keV range. Ikebe et al. (1996) point out that the central excess of X-ray emission seen in the Fornax cluster shows the existence of another dark matter component which is distinct from that representing the gravitational potential of the whole cluster. That is, the dark matter in this cluster shows a double distribution. For the Centaurus cluster, Fukazawa et al. (1994) and Ikebe et al. (1999) show that the gas attributed to the central excess emission has at least two temperature components. Moreover, Xu et al. (1998) find that the central excess emission in A1795 is dominated by the hot component and not by the cold component. Although the two-temperature structure and/or central excess emission in many clusters have been interpreted in terms of cooling flows (Fabian 1994), it is valuable to study them statistically in terms of a double distribution of dark matter and compare the results for the central emission with those for the whole cluster. For example, if there are indeed two components of dark matter distribution in clusters, hierarchical clustering scenario predicts that the inner component collapsed before the outer component did according to the law of perturbation growing. The fundamental plane analysis of the inner components is done in §3.

The discrepancy of the cluster L_X - T relation has been studied by many authors. While a simple scaling theory predicts $L_X \propto T^2$ (Kaiser 1991; Eke et al. 1996), observations show that $L_X \propto T^3$ (e.g. Edge, Stewart 1991; Markevitch 1998). One interpretation of the discrepancy is that the entropy of the gas in all clusters is raised at early times to levels comparable to those reached through the gravitational collapse (Kaiser 1991; Evrard, Henry 1991). As a result, the central density has an upper limit; in particular, the clusters with low temperature are severely affected by the limit. Indeed, Ponman et al. (1999) find that the entropy of the intracluster gas is higher than can be explained by gravitational collapse

alone, especially for poor clusters (see also David et al. 1996). They argue that the excess entropy is a relic of the energetic winds generated by supernovae in the forming galaxies. While Ponman et al. (1999) investigate the entropy outside the core region, in §4 we investigate that in the central region of clusters where the information of cluster formation is expected to be kept although cooling is effective.

The final issue in this paper is the metal abundance. The metal abundance of clusters is useful to know the chemical evolution of clusters and a possible correlation with dynamical quantities is a very interesting subject. ASCA has revealed the metal abundance distribution in clusters. Although the iron abundance outside the core region is roughly 1/3 solar and it is universal (Renzini 1997; Fukazawa 1998), some clusters have abundance excess (especially in iron) within the core region (Fukazawa 1997). However, not all clusters have the excess, and what makes the variation in the abundance excess is not well understood. Metals are ejected from galaxies in a cluster. Since the spatial distribution of galaxies in a cluster is more centrally concentrated than that of intracluster gas, and since a giant cD galaxy is situated at the center for most clusters, it is natural to expect that the metal abundance distribution has a central excess (Fujita, Kodama 1995; Ezawa et al. 1997). Thus, the non-existence of the abundance excess in some clusters may imply a mechanism to deform the original abundance distribution. However, the mechanism for this is still unknown. Fukazawa (1997) shows that the correlation between temperature of clusters and metal abundance at the centers is weak, while Allen and Fabian (1998) indicate that clusters with cooling flows tend to have the abundance excess. In §5, we investigate the relation between the metal abundance at the center of clusters and the virial density.

Based on the above results, we discuss the evolution of the core region of clusters in §6. Section 7 is devoted to the conclusions. Throughout this paper, we assume $H_0 = 50 \text{ km s}^{-1} \text{ Mpc}^{-1}$.

2. Fundamental Plane Analysis with Einstein Data

In paper I, we found that clusters form a fundamental plane and band in the $(\log \rho_0, \log R, \log T)$ space, using ROSAT data of 45 clusters with $z \sim 0$ obtained by Mohr et al. (1999); the sample is nearly flux-limited. In this section, we show that the relations found in Paper I are also reproduced with Einstein data and prove that the relations, especially the one between ρ_0 and R , are not significantly affected by observational errors such as uncertainties in the treatment of a central excess in emission and a correction of point spread function of telescopes. We use Einstein data of ρ_0 and R for 46 X-ray clusters

with $z \sim 0$ obtained by Jones and Forman (1984), although it is not a complete sample. Twelve clusters overlap between the catalogue of Jones and Forman (1984) and that of Mohr et al. (1999). The densities and core radii are obtained by fitting surface brightness profiles by the conventional β model,

$$\rho_{\text{gas}}(r) = \frac{\rho_0}{[1 + (r/R)^2]^{3\beta/2}}, \quad (1)$$

where r is the distance from the cluster center and β is a fitting parameter. If a central excess in emission is seen, Jones and Forman (1984) excise the photon count data of the innermost region of the cluster, when they fit the surface brightness profiles to equation (1). Thus, the effect of local luminosity excess is excluded. On the other hand, Mohr et al. (1999) fit the excess with another β model instead of excising it, noting that in the way of Jones & Forman (1984), the best fit core radius is correlated with the size of the excised region and the result is rather subjective. But in this section, we simply follow the prescription of Jones & Forman (1984).

The data of temperature are taken from the ASCA data catalogues if the clusters are observed by ASCA (17 clusters; Fukazawa et al. 1998; Markevitch 1998). Since not all clusters in the catalogue of Jones & Forman (1984) are observed by ASCA, the rest is taken from the catalogue of White, Jones, & Forman (1997), where they derived the temperatures using Einstein data by the deprojection method (Fabian et al. 1981). Although in paper I, we used the temperature data of previous ASCA, Ginga and Einstein observations gathered by Mohr et al. (1999), no significant difference in the results is found by this choice.

As

in Paper I, the data plotted in the $(\log \rho_0, \log R, \log T)$ space are fitted with a plane,

$$A \log \rho_0 + B \log R + C \log T + D = 0. \quad (2)$$

The result of the least square fitting with equal weight for simplicity is $A : B : C = 1 : 1.40 : -1.48$. The scatter about the plane is 0.08 dex. In paper I, we obtained the result of $A : B : C = 1 : 1.39 : -1.29$ with a scatter about the plane of 0.06 dex. The scatters are nearly equal to typical observational uncertainties. Thus, the existence of the ‘fundamental plane’ is also confirmed for the Einstein data, and it is consistent with the ROSAT data. From now on, we sometimes represent Einstein and ROSAT results with indices E and R, respectively.

In order to study the distribution of the observational data on the fundamental plane, we fit the data to another plane.

$$a \log \rho_0 + b \log R + c \log T + d = 0, \quad (3)$$

under the constraint,

$$Aa + Bb + Cc = 0. \quad (4)$$

This means that the plane (3) is perpendicular to the fundamental plane (2). The result is $a_E : b_E : c_E = 1 : 1.81 : 2.38$. The scatter about the plane is 0.2 dex. In paper I, we found that $a_R : b_R : c_R = 1 : 1.18 : 2.04$, with a scatter about the plane of 0.2 dex. We call this plane ‘the vertical plane’. Two unit vectors perpendicular to the fundamental and vertical planes are respectively defined by

$$\mathbf{e}_1 = \frac{1}{\sqrt{A^2 + B^2 + C^2}}(A, B, C), \quad (5)$$

$$\mathbf{e}_2 = \frac{1}{\sqrt{a^2 + b^2 + c^2}}(a, b, c). \quad (6)$$

For Einstein data, \mathbf{e}_1 , \mathbf{e}_2 , and one of the unit vectors perpendicular to them \mathbf{e}_3 are respectively given by

$$\mathbf{e}_{1E} = (0.44, 0.62, -0.65), \quad (7)$$

$$\mathbf{e}_{2E} = (0.32, 0.57, 0.76), \quad (8)$$

$$\mathbf{e}_{3E} = (0.84, -0.54, 0.057). \quad (9)$$

For comparison, the ROSAT data give

$$\mathbf{e}_{1R} = (0.47, 0.65, -0.60), \quad (10)$$

$$\mathbf{e}_{2R} = (0.39, 0.46, 0.80), \quad (11)$$

$$\mathbf{e}_{3R} = (0.79, -0.61, -0.039) \quad (12)$$

(Paper I). Since the observational uncertainty of each component of vectors is ~ 0.1 , the sets of vectors (7)–(9) and (10)–(12) are consistent with each other. For Einstein data, the equations $X_E = \rho_0^{0.44} R^{0.62} T^{-0.65}$, $Y_E = \rho_0^{0.32} R^{0.57} T^{0.76}$, and $Z_E = \rho_0^{0.84} R^{-0.54} T^{0.057}$ are three orthogonal quantities. Similarly, for ROSAT data, $X_R = \rho_0^{0.47} R^{0.65} T^{-0.60}$, $Y_R = \rho_0^{0.39} R^{0.46} T^{0.80}$, and $Z_R = \rho_0^{0.79} R^{-0.61} T^{-0.039}$ are three orthogonal quantities. Figure 1a shows the cross section of the fundamental plane viewed from the Y_E axis, while figure 1b shows the data on the (Y_E, Z_E) plane. These figures correspond to figures 1 and 2 in Paper I, respectively. As can be seen, a clear correlation (‘fundamental band’) exists on the plane.

We compare the relations among physical quantities based on Einstein data with those based on ROSAT data. The vector \mathbf{e}_{3E} , which corresponds to the major axis of the fundamental band, means that

$$\rho_0 \propto R^{-1.6 \pm 0.3}, \quad (13)$$

and

$$T \propto R^{-0.1 \pm 0.2} \propto \rho_0^{0.07 \pm 0.1}. \quad (14)$$

These relations should be compared to the results of ROSAT data obtained in Paper I:

$$\rho_0 \propto R^{-1.3 \pm 0.2}, \quad (15)$$

and

$$T \propto R^{0.06 \pm 0.1} \propto \rho_0^{-0.05 \pm 0.1}. \quad (16)$$

Thus, for both data sets, the major axis of the fundamental band is nearly parallel to the $\log \rho_0 - \log R$ plane, i.e., temperature varies very little along the fundamental band.

In paper I, we showed that the observed $L_X - T$ relation corresponds to a cross section of the fundamental plane. Moreover, we investigated the physical meaning of the observed $L_X - T$ relation. In the rest of this section, we show that the fundamental plane derived from the Einstein data has the same physical meaning as that derived from the ROSAT data. We here assume that the scatter around the fundamental plane is due to observational uncertainties alone, that is, $\Delta \log X_E$ (or $\Delta \log X_R$) is essentially zero. In this case, a physical quantity corresponding to each point on the fundamental plane can be represented by two parameters. For example, if we represent the gas mass fraction f with virial mass M_{vir} and density ρ_{vir} , the result turns out to be

$$f \propto M_{\text{vir}}^{0.4} \rho_{\text{vir}}^{-0.1}, \quad (17)$$

for the ROSAT data (Paper I). On the contrary, the analysis using the Einstein data results in

$$f \propto M_{\text{vir}}^{0.5} \rho_{\text{vir}}^{0.0}. \quad (18)$$

In relations (17) and (18), we assume the usual scaling relations $M_{\text{vir}} \propto RT$ and $\rho_{\text{vir}} \propto R^{-2}T$ for dynamical equilibrium. Since R is the core radius, M_{vir} and ρ_{vir} respectively represent the virial mass and density of the core, strictly speaking. Both (17) and (18) show that the observed $L_X - T$ relation can be interpreted as a relative paucity of gas in small clusters.

Since we have confirmed that the Einstein and ROSAT data give the same relationships, and since the spatial resolution of ROSAT is superior to that of Einstein, we use the ROSAT data in the following sections.

3. The Central Excess Emission

Up to now, we have concentrated on the outer components of surface brightness profile, but it is interesting to examine the nature of the inner components, or the central excess emissions when they exist. In this section, we extend the fundamental plane analysis to the inner components. In the catalogue of Mohr et al. (1999), the core radii R_{in} and the central gas densities of the inner components $\rho_{0,\text{in}}$ (R_2 and ρ_0 in their notation) are given. Although the emissions from the inner components include those from several temperature components, in most cases they are dominated by the emission from higher temperature components whose temperatures nearly equal to the average temperatures of the

clusters (Tamura et al. 1996; Xu et al. 1997, 1998; Ikebe et al. 1997). Thus, we here assume that emission from the inner components is totally from the higher temperature components. In fact, Mohr et al. (1999) assumed that the clusters are isothermal when they derive R_{in} and $\rho_{0,\text{in}}$. We later discuss the uncertainties of this assumption. For the temperature of the inner and outer components, we use spatially averaged temperature T_{av} presented by Mohr et al. (1999). In figure 2, we lap the data of the inner components over figures 1 and 2 in Paper I. The definitions of the axes are the same as those in Paper I. The data of inner components are situated on the fundamental plane.

We consider more quantitatively the band distribution as we did in Paper I and §2. We fit the combined data including those of the inner components to equations (2) and (3). When the combined data of Paper I and those of inner components are fitted, the unit vectors perpendicular or parallel to the planes are

$$\mathbf{e}_{1\mathbf{I}} = (0.43, 0.60, -0.68), \quad (19)$$

$$\mathbf{e}_{2\mathbf{I}} = (0.46, 0.50, 0.74), \quad (20)$$

$$\mathbf{e}_{3\mathbf{I}} = (0.78, -0.63, -0.058), \quad (21)$$

where index I represents the sample including the inner components. We may define $X_{\mathbf{I}}$, $Y_{\mathbf{I}}$, and $Z_{\mathbf{I}}$ from equations (19)–(21) in the same way as X_E , Y_E , and Z_E . Taking account of the fact that observational uncertainties of each component of the vectors are typically ~ 0.1 , equations (19)–(21) are consistent with equations (10)–(12). Thus, the data of the inner components satisfy the relations of the fundamental plane and band we found in Paper I, that is, satisfy the same relations as those among physical properties of the outer components. Figure 2 shows that the values of X_R and Y_R of the inner components are not much different from those of the outer components. However, the values of Z_R of the inner components are significantly larger than that of the outer components, because $\rho_{\text{vir}} (\propto R^{-2}T)$ and ρ_0 of the inner components are larger.

It is to be noted that there may be systematic errors in the data we used, because we have used the values of the gas density and core radius derived on the assumption that clusters are isothermal. Recently, the structure of the intracluster gas at the cluster centers is investigated in detail with ASCA for several clusters. When a cluster has two components in the surface brightness distribution, the inner component often has two temperatures of $\gtrsim 3$ keV and ~ 1.5 keV (e.g. Centaurus cluster; Ikebe et al. 1999). The detailed observations show that the hot and cold components coexist in the core (e.g. Fukazawa 1994; Ikebe et al. 1999). Moreover, spatially resolved temperature profiles obtained by ASCA indicate that the temperature of the hot components is nearly equal to

T_{av} (Fukazawa 1994; Xu et al. 1998; Ikebe et al. 1999). Thus, the assumption of isothermality is correct when the emission from the inner component is dominated by the one from the hot component. In fact, for clusters such as A1060 (Tamura et al. 1996), AWM7 (Xu et al. 1997), Hydra-A (Ikebe et al. 1997), and A1795 (Xu et al. 1998), the emissions from the centers are dominated by those from the hot components. On the other hand, for some clusters, such as Centaurus, both emissions from the hot and cold components comparably contribute to the central emission excess, although the hot component dominates in volume. Ikebe et al. (1999) investigate the central region of the Centaurus cluster in detail; they determine $\rho_{0,\text{in}}$ and R_{in} of the Centaurus cluster by the analysis combining the ASCA and ROSAT data. They distinguish $\rho_{0,\text{in}}$ and R_{in} for the hot components from those of the cold components in the central region. Moreover, they take account of the inhomogeneity of metal abundance contrary to the analysis by Mohr et al. (1999). They find that $\rho_{0,\text{in}} \sim 0.02 \text{ cm}^{-3}$ and $R_{\text{in}} = 46 \text{ kpc}$ for the hot component, and that $\rho_{0,\text{in}} \sim 0.06 \text{ cm}^{-3}$, $R_{\text{in}} = 12 \text{ kpc}$ for the cold component. The data obtained by Mohr et al. (1999) are consistent with those for the cold component but not for the hot component. This indicates that there exist systematic errors of factor 4 in $\rho_{0,\text{in}}$ and R_{in} of the inner component in this cluster. (It should be noted that even if the data obtained by Ikebe et al. (1999) are used, the data of inner hot component of the Centaurus cluster are still on the fundamental plane as is shown in figure 2.)

However, the Centaurus cluster seems to be the most extreme case. Among the clusters whose central regions are closely observed by ASCA (Centaurus, Virgo, A1060, AWM7, Hydra-A, A1795, and Fornax), the Centaurus cluster has the strongest abundance gradient. Moreover, only Centaurus and Virgo (Matsumoto et al. 1996) have the X-ray emission from the cold components comparable to the hot components. Furthermore, the central emission of the Centaurus cluster is situated on the high Z_{R} end of the fundamental band (figure 2), while those of A1060 and others are not. Since ρ_0 of clusters at this end is large and the cooling time of the intracluster gas is short, the clusters are expected to have strong emissions from the cold components. Thus, we conclude that *for most clusters we investigated, the hot components dominate the central excess emissions and the excesses are related to the fundamental band.* Therefore, for most clusters, the systematic errors of the inner components should be smaller than those of the Centaurus cluster. Future observations will clarify this point.

4. Entropy

The entropy of intracluster gas is intimately related to the thermal history of the cluster. Virialization of a

cluster at the formation and additional heating processes produce the entropy. Ponman et al. (1999) investigated the intracluster gas at a certain radius outside core region where radiative cooling is not effective. They fix the radius at 0.1 times the present virial radius (r_{01}), thus taking a nearly fixed value of ρ_{gas} . They find that hot clusters satisfy the relation,

$$S_{\text{gas}} = \log T + \text{const} , \quad (22)$$

which would be satisfied when gravitational collapse alone produces the entropy and when the profiles of gas density are similar, while cool ($T < 4 \text{ keV}$) clusters does not. Moreover, they find that the entropy has a minimum value ($\sim 100 \text{ keV cm}^2$), which they call the ‘entropy floor’ for cool clusters. They suggested that the floor is a relic of the energetic galactic winds before the cluster formation.

On the other hand, since the gas is affected by cooling in the core region of clusters, we expect that the entropy there provides information about not only heating but also cooling. Following the study of Ponman et al. (1999), we first consider the relation between the entropy and temperature of gas at the center of clusters. The entropy of the gas at the cluster center is given by

$$S_{\text{gas}} = \log(\rho_0^{-2/3} T) + \text{const} , \quad (23)$$

where ρ_0 is the central gas density derived by β fitting (Mohr et al. 1999). If a cluster has two components in the surface brightness distribution, we discriminate between ρ_0 of the inner components and that of the outer components by index in and out, respectively. Since Mohr et al. (1999) do not present gas densities of the outer components $\rho_{0,\text{out}}$, we give them by

$$\rho_{0,\text{out}} = \left(\frac{I_{\text{out}} R_{\text{in}}}{I_{\text{in}} R_{\text{out}}} \right)^{1/2} \rho_{0,\text{in}} , \quad (24)$$

where I_{out} and I_{in} are the central surface brightnesses corresponding to the outer and the inner components, respectively, and R_{out} is the core radius of the outer component.

Figure 3a shows the relation between the entropy and temperature of gas at the center of clusters. Contrary to the result of Ponman et al. (1999), it has a large scatter. This is because not only T but also ρ_0 varies; ρ_0 takes a wide range of values in comparison with the gas density at r_{01} . Most of the variation of ρ_0 reflects that of ρ_{vir} (Paper I), that is, the formation redshift of the cluster. Thus, our method enables us to treat the relation between the entropy and the cluster formation redshift in contrast of Ponman et al. (1999). In order to investigate the relation, we consider the relation between S_{gas} and ρ_{vir} . The density of ρ_{vir} is assumed to be proportional to $R^{-2} T$, where R and T are the core radius and temperature of the cluster, respectively, thus represented in the

units of keV Mpc⁻². If a cluster has two components in the surface brightness distribution, we use the core radii of the components R_{in} and R_{out} , respectively, and we use the common temperature T_{av} . The data are taken from Mohr et al. (1999).

Figure 3b shows the relation between ρ_{vir} and S_{gas}^* ($= 10^{S_{\text{gas}}}$). As can be seen, the variation of S_{gas}^* is related to that of ρ_{vir} . Moreover, the correlation is tight. This may mean that in the central region of clusters, the inner component prescribes the structure and evolution of intracluster gas. We fit the points in Figure 3a and 3b to the following plane,

$$S_1 \log \rho_{\text{vir}} + S_2 \log T + S_3 \log S_{\text{gas}}^* + S_4 = 0. \quad (25)$$

The result is $(S_1, S_2, S_3) = (-0.4, 0.9, -1)$, that is,

$$S_{\text{gas}} = \log(\rho_{\text{vir}}^{-0.4 \pm 0.1} T^{0.9 \pm 0.3}) + \text{const}. \quad (26)$$

Equation (25) is a linear transformation of the fundamental plane including the inner components (eqs.[19]-[21]), because this is nothing but the relation among ρ_0 , R , and T . Indeed, if we use the relation (17), which is equivalent to the fundamental plane in the $(\log \rho_0, \log R, \log T)$ space, we obtain

$$S_{\text{gas}}^* \propto \frac{T}{\rho_{\text{gas}}^{2/3}} \propto \frac{T}{(f \rho_{\text{vir}})^{2/3}} \propto \frac{T}{M_{\text{vir}}^{4/15} \rho_{\text{vir}}^{0.6}} \propto \frac{T^{3/5}}{\rho_{\text{vir}}^{7/15}}. \quad (27)$$

This is nearly equivalent to the equation (26). We can represent S_{gas}^* , ρ_{vir} , and T by X_{I} , Y_{I} , and Z_{I} , which correspond to equations (19)-(21),

$$S_{\text{gas}}^* \propto X_{\text{I}}^{-1.0} Y_{\text{I}}^{0.4} Z_{\text{I}}^{-0.6}, \quad (28)$$

$$\rho_{\text{vir}} \propto X_{\text{I}}^{-1.9} Y_{\text{I}}^{-0.3} Z_{\text{I}}^{1.2}, \quad (29)$$

$$T \propto X_{\text{I}}^{-0.7} Y_{\text{I}}^{0.7} Z_{\text{I}}^{-0.1}. \quad (30)$$

Since the scatters of X_{I} , Y_{I} , and Z_{I} are $\Delta \log X_{\text{I}} = 0.07$, $\Delta \log Y_{\text{I}} = 0.2$, and $\Delta \log Z_{\text{I}} = 0.6$, respectively, the variations of S_{gas}^* and ρ_{vir} are mainly due to that of Z_{I} . Thus, figure 3b nearly corresponds to figure 2a or a side view of the fundamental plane, because the difference between Z_{R} and Z_{I} is small. Note that the relatively large uncertainty in the power of T in equation (26) and the slight difference of T -dependence between equations (26) and (27) come from the fact that the scatter around the plane $\Delta \log X_{\text{I}}$, which corresponds to observational uncertainty, is emphasized by the linear transformation, because $S_{\text{gas}}^*/\rho_{\text{vir}}^{-0.4} \propto X_{\text{I}}^{-1.7} Y_{\text{I}}^{0.3} Z_{\text{I}}^{-0.1}$.

The line in figure 3b is the gas entropy achievable through gravitational collapse alone ($S_{\text{gas}}^* \propto \rho_{\text{vir}}^{-2/3}$ for a given T). The normalization of the line is adjusted to the clusters with small ρ_{vir} , because the influences of additional heating and cooling are expected to be small for them. The observed entropies of large ρ_{vir} clusters are located above the line. This is because of the non-constant

f (relation [27],[17]), that is, the central gas fraction of poor clusters (generally having large ρ_{vir}) is smaller than that of rich clusters. Although the gas entropy at the cluster centers is larger than achievable through gravitational collapse alone for large ρ_{vir} clusters, it does not converge to a floor value, contrary to the result of Ponman et al. (1999). This means that the cooling is effective in the central region of the clusters.

5. Metal Abundance

In this section, we study the relation between central metal abundance and ρ_{vir} . Since there is a giant cD galaxy at the center of most clusters, the metal abundance at the cluster center may mainly reflect the interstellar medium and the chemical evolution of the cD galaxy. We study 22 clusters overlapping in the catalogues of Mohr et al. (1999) and Fukazawa (1997). We investigate the iron abundance $Z_{\text{Fe,in}}$ and the silicon abundance $Z_{\text{Si,in}}$ for the central region (here subscript ‘in’ donates the central value rather than the inner components). The data of metal abundance are taken from Fukazawa (1997). We treat the inner component if a cluster has two components in the surface brightness distribution, as well as the clusters for which a single component fit is acceptable. As we did in the previous sections, we assume that clusters are isothermal. However, for clusters with relatively strong emission from the cold component at the cluster center, the data may suffer from systematic errors as discussed in §3. For example, the Centaurus cluster should have ρ_{vir} between the two data in figure 4a, because the core radius of the inner component of the cluster derived by Mohr et al. (1999) nearly equals to that of the cold component (see. §3).

Figure 4a shows that $Z_{\text{Fe,in}}$ is an increasing function of ρ_{vir} , while $Z_{\text{Si,in}}$ reveals no clear tendency. The correlation between $Z_{\text{Fe,in}}$ and ρ_{vir} indicates that our arguments about the fundamental relations among ρ_0 , R , and T are physically meaningful. If the range of variation $\rho_{\text{vir}} \propto R^{-2} T$ were due to an observational inaccuracy of R , the correlation between $Z_{\text{Fe,in}}$ and ρ_{vir} would not exist. Although the data of silicon abundance have a large scatter (~ 0.5 solar, figure 4a), the silicon to iron abundance ratio $Z_{\text{Si,in}}/Z_{\text{Fe,in}}$ is a decreasing function of ρ_{vir} (figure 4b). Since iron and silicon are supposed to be supplied by different sources (Type Ia and II supernovae, respectively), this correlation suggests that the contribution of Type Ia SNe is larger for clusters with larger ρ_{vir} , while that of type II SNe is more or less the same for all clusters.

6. Discussion

In §3, we find that for clusters with a double surface brightness profile, the inner components satisfy the same

relations of the fundamental plane and band as those of the outer emission components. One possible interpretation is that the inner and outer emission components correspond to the separate dark matter components collapsed at different epochs under a hierarchical clustering scenario, and that the temperature of the inner hot component represents the depth of the potential well of the inner dark matter component as suggested by recent ASCA observations. Assuming that the core of a cluster forms when a major merger (we simply say ‘collapse’, hereafter) occurs and that the envelope grows through minor mergers or accretion after that (e.g. Salvador-Solé et al. 1998), the interpretation implies that the collapse has occurred at least twice in the cluster with two components in the surface brightness distribution. In other words, the inner component of dark matter formed by the first collapse and had grown through accretion; when the second collapse occurs, the outer component of dark matter formed, and the cluster has grown further through accretion. In this scenario, the inner component of dark matter has survived the second collapse. In figure 5, we predict the formation epoch of each component of clusters using the spherical collapse model (Tomita 1969; Gunn, Gott 1972, see Paper II). As is seen, for a cluster with double distribution in the surface brightness, the inner component formed at $z \sim 4$ ahead of the formation of the outer component regardless of cosmological parameters; the outer component forms at $z \sim 0 - 0.5$. Since the gravitational mass is proportional to RT , figure 5b shows that the gravitational mass of the inner component is about 1% of that of the outer component. This implies that the clusters had already grown up to 1% of their present masses at $z \sim 4$. These may be consistent with the recent suggestion of Loken et al. (1999) and Miller et al. (1999) that clusters with central excess emissions reside in high density region of the Universe and started to collapse early.

Figure 3b shows that the gas entropy at the center of large ρ_{vir} clusters is larger than achievable through gravitational collapse alone (the line in figure 3b). On the other hand, figure 3b shows that, the gas entropy of large ρ_{vir} clusters is smaller than the ‘entropy floor’ ($\sim 100 \text{ keV cm}^2$) claimed by Ponman et al. (1999). If the intracluster gas was heated by galactic processes, as a result of which the entropy floor was established before the cluster formation as claimed by Ponman et al. (1999), our results suggest that the radiative cooling becomes effective at the center of these clusters after they collapse, but that it is not so effective to cancel out the initial heating in spite of the short cooling time of the gas at the cluster center ($\lesssim 10^9 \text{ yr}$), which is well below the cluster age. Thus, heating sources should exist in the central region of the cluster even after the cluster formed. Considering the fact that the band distribution in figure 3b is tight and all kinds of components are lo-

cated on the same band, the source must be stable and related to the evolution of the whole cluster. If the heating process is temporary and local, the points in figure 3b would not form a band.

From the above arguments, we may reject heating from the cosmic ray from AGN as the energy source, because the duration of the AGN activity is very short ($\sim 10^8 \text{ yr}$) and it cannot supply energy constantly. In fact, not all clusters have AGNs at the centers. Moreover the energy loss time of cosmic ray particles is well below the cluster age (e.g. Rephaeli, Silk 1995). Although supernovae seem to be more stable energy sources, the amount of energy is insufficient. For elliptical galaxies, which dominate in the central region of clusters, the supernova rate is at most 0.1 per $10^{10} L_{\text{B}\odot}$ per 100 yr (Turatto et al. 1994), where $L_{\text{B}\odot}$ is the B-band solar luminosity. Since typical B-band luminosity of a cD galaxy is $\sim 10^{11} L_{\text{B}\odot}$, the heating rate of supernovae is $\sim 10^{42} \text{ erg s}^{-1}$, assuming that each supernova ejects the energy of 10^{51} erg . This is smaller than typical X-ray emission in the core region of a cluster ($\sim 10^{43-44} \text{ erg s}^{-1}$). Multi-phase cooling flow (Fabian 1994) and heat conduction (Takahara, Takahara 1979) may stably transport energy from outside region of a cluster, where high-entropy gas should be generated by shock heating through accretion (Mezler, Evrard 1994; Navarro et al. 1995). In particular, the former model may explain the existence of the cold components in the central region of clusters. However, for the former model, the ultimate fate of the cooled gas is still unexplained (e.g. McNamara, Jaffe 1994; Voit, Donahue 1995). For the latter model, a mechanism of local reduction of heat conductivity is needed. This is because the classical conduction rate is too large to allow the existence of the cold gas component (Sarazin 1986; Bregman, David 1988), while such a component certainly exists in the core regions of clusters (Ikebe et al. 1999; Fukazawa 1997). Therefore, there is no satisfactory model of the energy source or transmission so far.

In §5, we investigate the relation between metal abundance ($Z_{\text{Si,in}}$ and $Z_{\text{Fe,in}}$) and ρ_{vir} . Since iron is mainly produced by Type Ia SNe and silicon is mainly produced by Type II SNe, this reveals the difference between the history of Type Ia and Type II SNe rates. Figure 4a shows that there is no correlation between ρ_{vir} and $Z_{\text{Si,in}}$. This may indicate that most of Type II SNe occurred before the collapse of the central region of clusters. On the contrary, figure 4b shows that $Z_{\text{Si,in}}/Z_{\text{Fe,in}}$ is a decreasing function of ρ_{vir} . This decrease is chiefly attributed to the fact that the iron abundance excess is seen at the center of the clusters with large ρ_{vir} . This implies that the iron ejected from the galaxies at the cluster centers has accumulated in large ρ_{vir} and thus early collapsed clusters, although other possibilities cannot be ruled out. The clusters with $\rho_{\text{vir}} \gtrsim 10^3 \text{ keV Mpc}^{-2}$ especially have low silicon to iron abundance ratio (figure 4b). When

$\Omega_0 = 1$ ($\rho_{\text{vir}} \propto [1 + z]^3$), this means that the central iron abundance excess is observed only in the clusters which collapsed at $z > z_{\text{Fe}} \sim 2 - 3$, assuming that the left end of the distribution ($\rho_{\text{vir}} \sim 20 \text{ keV Mpc}^{-2}$) corresponds to the clusters which collapse at $z \sim 0$. When a cluster collapses, we expect that the existing iron excess at the center is smoothed out because of some violent mixing processes of intracluster gas. Thus, the observational data may show that the iron had been ejected from Type Ia SNe into the intracluster gas at the cluster center for $z > z_{\text{Fe}}$, if the evolution of Type Ia SNe rate is universal. In other words, if a cluster collapsed at $z = z_{\text{coll}} > z_{\text{Fe}}$, the iron excess had grown again during $z_{\text{coll}} > z > z_{\text{Fe}}$, although it was once smoothed out at z_{coll} . On the other hand, if clusters formed at $z < z_{\text{Fe}}$, little iron is supplied from Type Ia SNe after the formation and thus no iron excess is observed. Assuming that the galaxies in the clusters formed at $z \gg z_{\text{Fe}}$, these imply that the iron ejection had continued for the initial few Gyrs. The time-scale is roughly consistent with the theoretically predicted one (e.g. Mihara, Takahara 1994). This is almost the same for $\Omega_0 = 0.2$. Finally, we comment on the relation between cooling flows and the central abundance excess suggested by Allen and Fabian (1998). Since old clusters have compact and dense cores, their central gas density also tends to be large. Thus, the clusters satisfy the criterion of cooling flow, that is, the cooling time of gas is smaller than the Hubble time.

7. Conclusions

We consider the scaling relations of the core region of clusters using the X-ray data. We first confirm that the fundamental relations among central gas density, core radius, and temperature we found using ROSAT data are reproduced by Einstein data, too. This means that the relations, especially between density and core radius, are not significantly affected by observational errors such as uncertainties in exclusion of the central emission excess and a correction of point spread function. This result strengthens our interpretation that clusters form a two parameter family in terms of mass and virial density.

We find that the central excess in emission observed in many clusters also satisfies the fundamental relations. If the excess reflects the existence of the distinct dark matter component from the whole cluster as suggested by Ikebe et al. (1996), our result implies that the inner component collapsed ahead of the collapse of the whole cluster in the scenario of hierarchical clustering and that it represents the gravitational potential of the component.

Gas entropies at the centers of old clusters show that both cooling and heating affect the thermal evolution of the intracluster gas. Moreover, the relation between the entropy and the virial density suggests that stable energy

sources or stable energy transmission mechanisms should exist in the central region of clusters. The ratio of silicon to iron abundance at cluster centers is a decreasing function of the central virial density. This can be interpreted that the iron ejection from Type Ia supernovae had occurred mainly before $z \sim 2 - 3$.

The upcoming X-ray telescopes with high spatial and spectral resolution such as Candra, XMM, and ASTRO-E will be quite useful for detailing this kind of studies.

This work was supported in part by the JSPS Research Fellowship for Young Scientists.

References

- Allen S.W., Fabian A.C. 1998, MNRAS 297, L53
 Bregman, J.N., David, L.P. 1988, ApJ 326, 639
 David L.P., Jones C., Forman W. 1996, ApJ 473 692
 Edge A.C., Stewart G.C. 1991, MNRAS 252, 414
 Evrard A.E., Henry J.P. 1991 ApJ 383, 95
 Ezawa H., Fukazawa Y., Makishima K., Ohashi T., Takahara F., Xu H., Yamasaki N.Y. 1997, ApJL, 490, 33
 Fabian A.C. 1994, ARAA 32, 277
 Fabian A.C., Hu E.M., Dowie L.L., Grindlay J. 1981, ApJ 248, 47
 Fujita Y., Kodama H. 1995. ApJ 452, 177
 Fujita Y., Takahara F. 1999a, ApJL, 519, 51
 Fujita Y., Takahara F. 1999b, ApJL, 519, 55
 Fukazawa Y. 1997, PhD thesis, University of Tokyo
 Fukazawa Y., Makishima K., Tamura T., Ezawa H., Xu H., Ikebe Y., Kikuchi K., Ohashi T. 1998, PASJ 50, 187
 Fukazawa Y., Ohashi T., Fabian A.C., Canizares C.R., Ikebe Y., Makishima K., Mushotzky R.F., Yamashita K. 1994, PASJ 46, L55
 Gunn J.E., Gott J.R. 1972, ApJ 176, 1
 Ikebe Y., Ezawa H., Fukazawa Y., Hirayama M., Ishisaki Y., Kikuchi K., Kubo H., Makishima K. et al. 1996, Nature 379, 427
 Ikebe Y., Makishima K., Ezawa H., Fukazawa Y., Hirayama M., Honda H., Ishisaki Y., Kikuchi K. et al. 1997, ApJ 481, 660
 Ikebe Y., Makishima K., Fukazawa Y., Tamura T., Xu H., Ohashi T., Matsushita K. 1999, ApJ 525, 58
 Jones C. Forman W. 1984, ApJ 276, 38
 Kaiser N. 1991, ApJ 383, 104
 Loken C., Melott A.L., Miller C.J. 1999, ApJL, 520, 5
 Markevitch, M. 1998, ApJ 504, 27
 Matsumoto H., Koyama K., Awaki H., Tomida H, Tsuru T., Mushotzky R., Hatsukade I. 1996, PASJ 48, 201
 McNamara B.R., Jaffe W. 1994, A&A 281, 673
 Mihara K., Takahara F. 1994, PASJ 46, 447
 Miller C.J., Melott, A.L., Gorman, P. 1999, ApJL 526, 61
 Mohr J.J., Mathiesen B., Evrard A.E. 1999, ApJ 517, 627
 Navarro J.F., Frenk C.S., White S.D.M. 1995, MNRAS 275, 720
 Navarro J.F., Frenk C.S., White S.D.M. 1997, ApJ 490, 493
 Ponman T.J., Cannon D.B., Navarro J.F. 1999, Nature 397, 135

- Renzini A. 1997, ApJ 488, 35
 Rephaeli, Y., Silk, J. 1995 ApJ 442, 95
 Salvador-Solé E., Solanes J.M., Manrique A. 1998, ApJ 499, 542
 Sarazin C.L. 1986, Rev. Mod. Phys. 58, 1
 Takahara M., Takahara F. 1979, Prog. Theor. Phys. 62, 1253
 Tamura T., Day, C.S., Fukazawa Y., Hatsukade I., Ikebe Y., Makishima K., Mushotzky R.F., Ohashi T. 1996, PASJ 48, 671
 Tomita K. 1969, Prog. Thor. Phys. 42, 9
 Turatto M., Cappellaro E, Benetti S. 1994, AJ 108, 202
 Voit G.M., Donahue M. 1995, ApJ 452, 164
 White D.A., Jones C., Forman W. 1997, MNRAS 292, 419
 Xu, H., Ezawa H., Fukazawa Y., Kikuchi K., Makishima K., Ohashi T., Tamura T. 1997, PASJ 49, 9
 Xu H., Makishima K., Fukazawa Y., Ikebe Y., Kikuchi K., Ohashi T., Tamura T. 1998, ApJ 500, 738

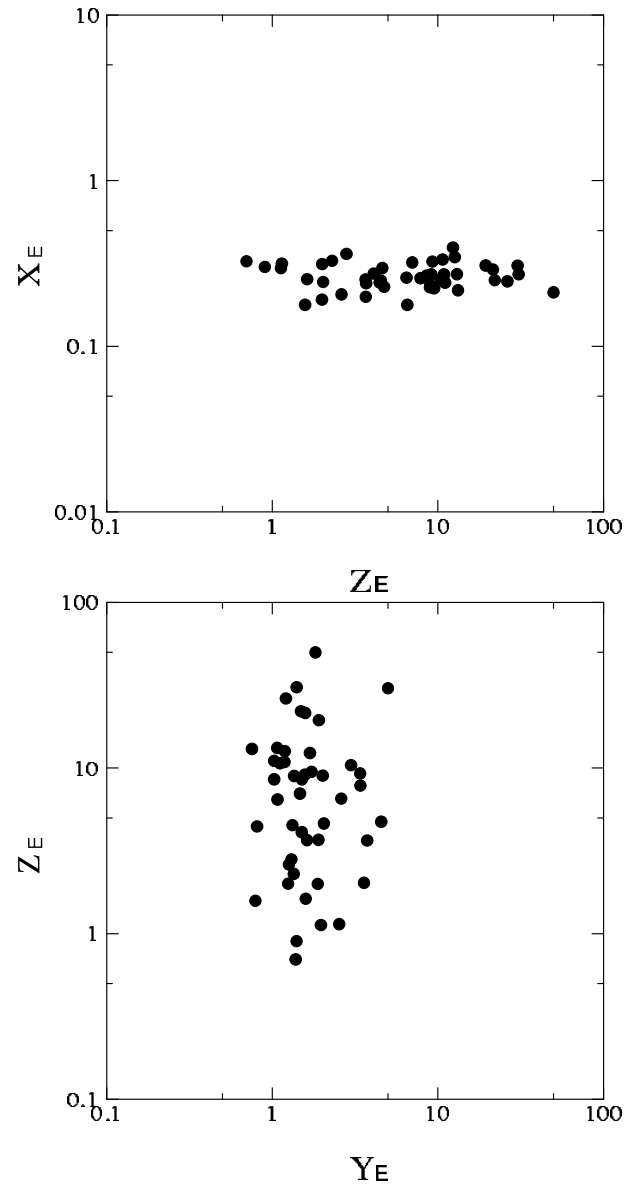


Fig. 1.. The observational data projected (a) on the $Z_E - X_E$ plane, (b) on the $Y_E - Z_E$ plane.

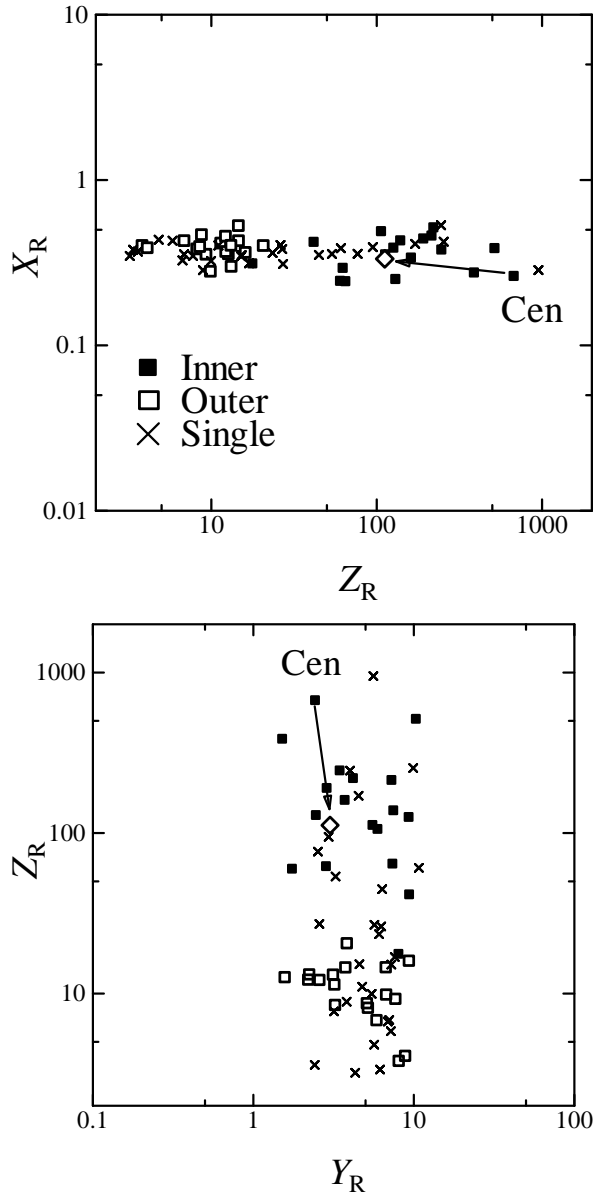


Fig. 2. The observational data projected (a) on the $Z_R - X_R$ plane, (b) on the $Y_R - Z_R$ plane. Filled squares, open squares, and crosses represent the inner components, the outer components, and the clusters without double distribution of surface brightness distribution, respectively. A diamond shows the hot inner component of the Centaurus cluster obtained by Ikebe et al. (1999).

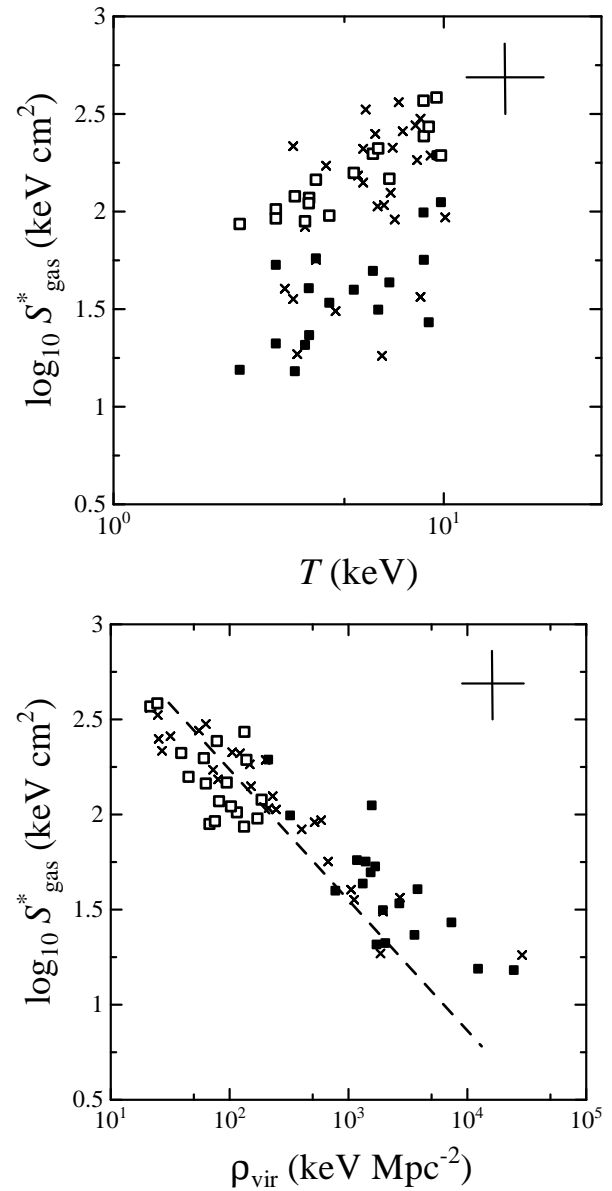


Fig. 3. The gas entropy at the cluster center as a function of (a) temperature of the cluster and (b) central virial density. Symbols are the same as those in figure 2. A typical error bar is shown at the upper right of the figures. A dashed line in figure 3b is proportional to $\rho_{\text{vir}}^{-2/3}$.

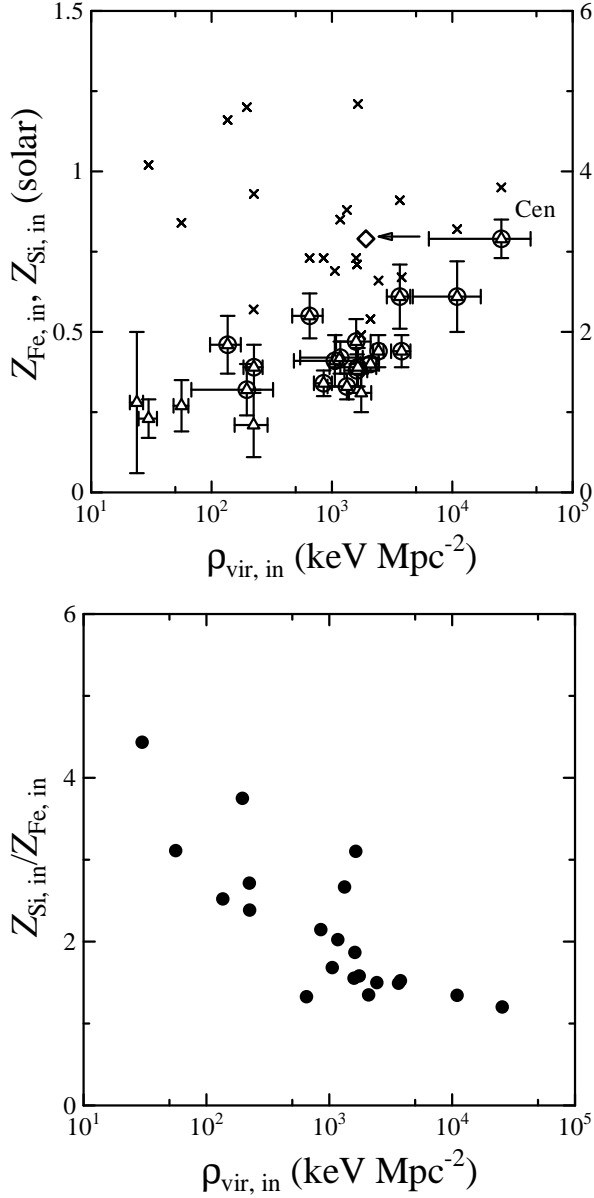


Fig. 4.. (a) The metal abundance at the cluster center as a function of central virial density of the cluster. In figure 4a, triangles and crosses represent $Z_{\text{Fe, in}}$ and $Z_{\text{Si, in}}$, respectively. The point of iron abundance with an open circle represents the cluster with a cD galaxy (Fukazawa 1997). The uncertainties of $Z_{\text{Si, in}}$ are typically 0.5 solar. A diamond shows the hot inner component of the Centaurus cluster obtained by Ikebe et al. (1999). (b) The abundance ratio $Z_{\text{Si, in}}/Z_{\text{Fe, in}}$ is represented as a function of central virial density of the cluster.

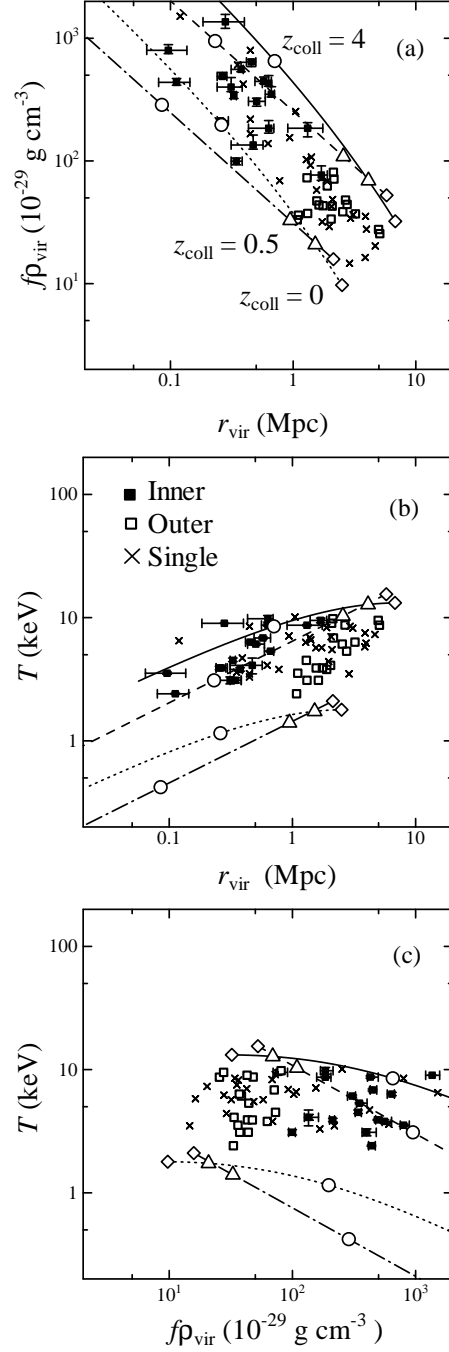


Fig. 5.. Theoretical predictions. (a) Radius–density relation (b) radius–temperature relation (c) density–temperature relation. Solid line: $\Omega_0 = 0.2$ and $M_{\text{vir}}(t_0) = 10^{16} M_{\odot}$. Dotted line: $\Omega_0 = 0.2$ and $M_{\text{vir}}(t_0) = 5 \times 10^{14} M_{\odot}$. Dashed line: $\Omega_0 = 1.0$ and $M_{\text{vir}}(t_0) = 10^{16} M_{\odot}$. Dash-dotted line: $\Omega_0 = 1.0$ and $M_{\text{vir}}(t_0) = 5 \times 10^{14} M_{\odot}$. The open diamonds, triangles, and circles correspond to the collapse redshifts of $z_{\text{coll}} = 0$, $z_{\text{coll}} = 0.5$, and $z_{\text{coll}} = 4$, respectively. The observational data (ρ_0 , R , and T) are overlaid being shifted moderately in the directions of ρ_0 and R ($f\rho_{\text{vir}} = 0.06\rho_0$ and $r_{\text{vir}} = 8R$). Filled squares, open squares, and crosses represent the inner components, the outer components, and the clusters without double distribution of the surface brightness, respectively. The error bars of the last two are omitted but presented in Paper I.